# THE LARGE SOLAR VACUUM TELESCOPE: THE OPTICAL SYSTEM, AND FIRST SPECTRAL OBSERVATIONS

V. I. SKOMOROVSKY and N. M. FIRSTOVA
*Institute of Solar-Terrestrial Physics, 664033 Irkutsk, P.O. Box 4026, Russia*

(Received 17 January, 1995; in revised form 17 July, 1995)

**Abstract.** The performance of the optics of the Large Solar Vacuum Telescope (LSVT) and examples of the spectrograms taken with the spectrograph are presented. A new pneumo-mechanical support system for the siderostat mirror and monitoring system of the telescope optics is described.

## 1. Introduction

The Large Solar Vacuum Telescope (LSVT) (Stepanov, Banin, and Kruglov, 1979) is situated on the shore of Lake Baikal (Figure 1). Its one-mirror tracking system, polar siderostat (Kruglov *et al.*, 1980) on a 25 m high metal column, reflects sunlight along the polar axis direction (latitude 52°) to a 760 mm aperture, 40 m focal length crown-flint doublet objective lens. The metal tank of the telescope is evacuated and sealed at the entrance crown window located between the main ceramic glass mirror and the objective lens on the top of the inclined column and the 1-m diameter exit crown window close to the ground level.

The 40 cm diameter solar image passing through the lower window is used for the scanning and guiding systems. There are two small sealed lateral glass windows for illumination of the spectrograph and an optical bench with narrow bandpass filters. The telescope has been operating since 1980 in different versions. The entire optical (Domyshev *et al.*, 1982) and mechanical system was produced at the Institute of Solar-Terrestrial Physics.

## 2. Optics of the Telescope

The assembled objective was tested by means of a laser interferometer in a laboratory vacuum tank. Interferograms of the siderostat mirror and a map of fractions of $\lambda$6328 Å of the objective wavefront with that mirror are shown in Figures 2 and 3, respectively. The objective concentrates 76% of the energy in a disk of $0.42''$ corresponding to the first diffraction maximum. The theoretical concentration is 82%. A disk of $1''$ diameter contains 92% of the energy against 94% for an ideal objective.

The surface of the entrance window was figured to almost five-wavelength of relief to compensate inhomogeneity. The pattern in Figure 4 was taken with a reference spherical mirror. The entrance window was still in production when the

*Solar Physics* **163:** 209–222, 1996.

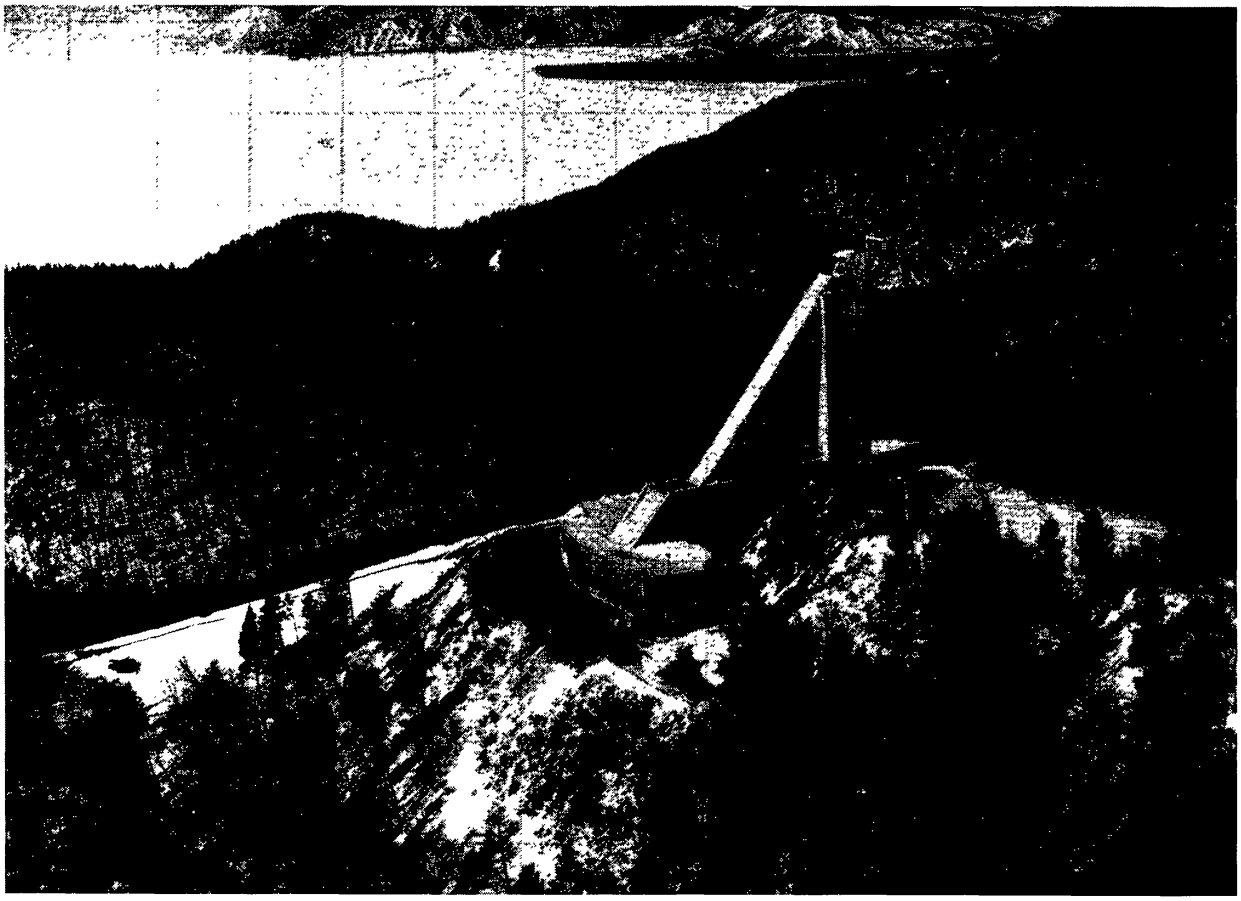

Fig. 1. The Large Vacuum Solar Telescope. Lake Baikal is visible in the background.

objective was installed on the telescope for a non-vacuum version, so we calculated the summary wavefront of the main mirror, entrance window and the objective for their best mutual position (Figure 5). This summary wavefront is the best that we can achieve with the telescope in real time during good seeing.

## 3. Testing Optical System

To control parameters of the optical system, the temperature gradients and the wavefront, three interferometers were installed on the telescope (Figure 6).

The upper interferometer uses a reflection from the outward convex surface of the positive lens of the objective. By monitoring the real-time change of the image of the interferogram, which depends on the temperature gradients in the lens glass, we can decide if the objective is good or not for observations.

To check the temperature gradients in the entrance window glass, we monitor with the low camera the interference pattern between the flat surfaces of the window. To perform such control, the objective is used like a collimator to take autocollimation images of the laser light source from both surfaces of the window. There is a small wedge between two surfaces to get 20–25 fringes on the

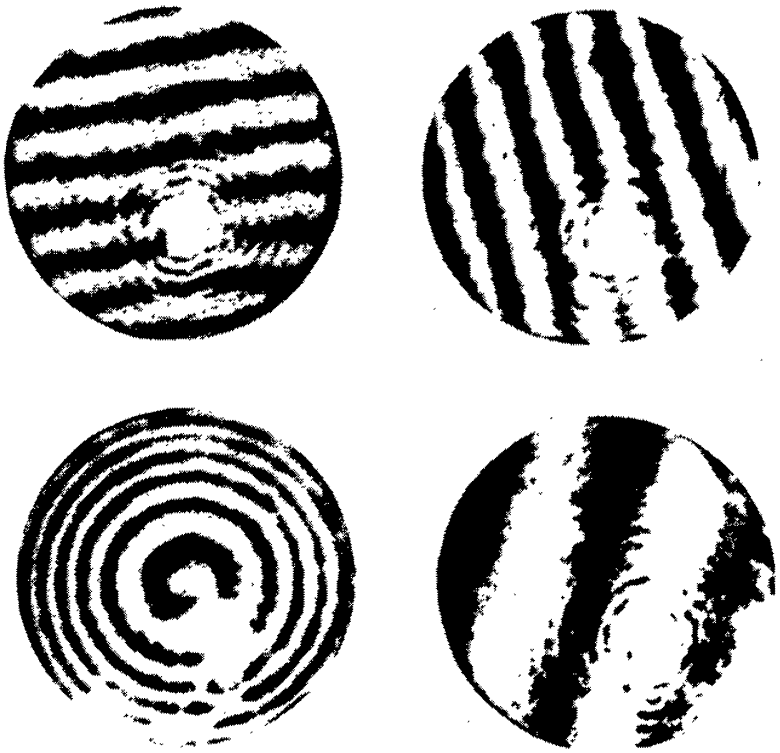

Fig. 2. Siderostat mirror interferograms.

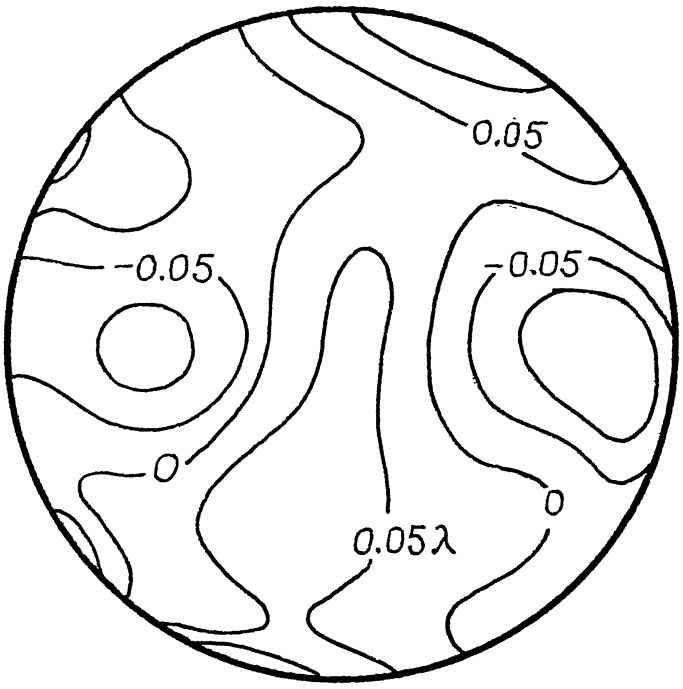


Fig. 3. Objective lens wavefront.

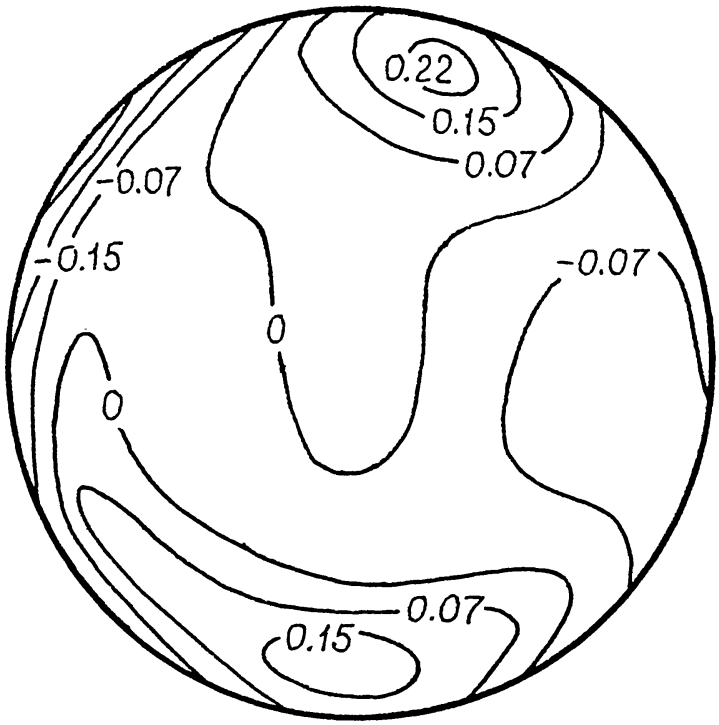


Fig. 4. Entrance window wavefront.

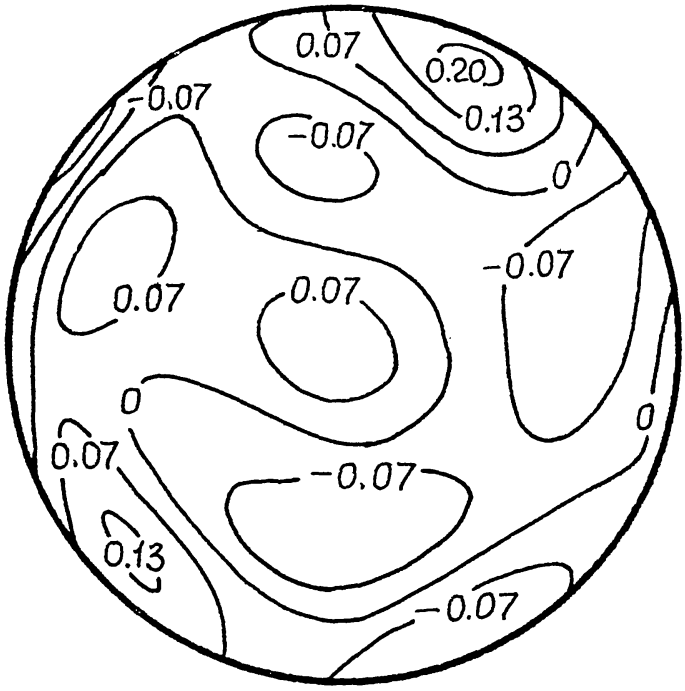


Fig. 5. Summary wavefront (calculation).

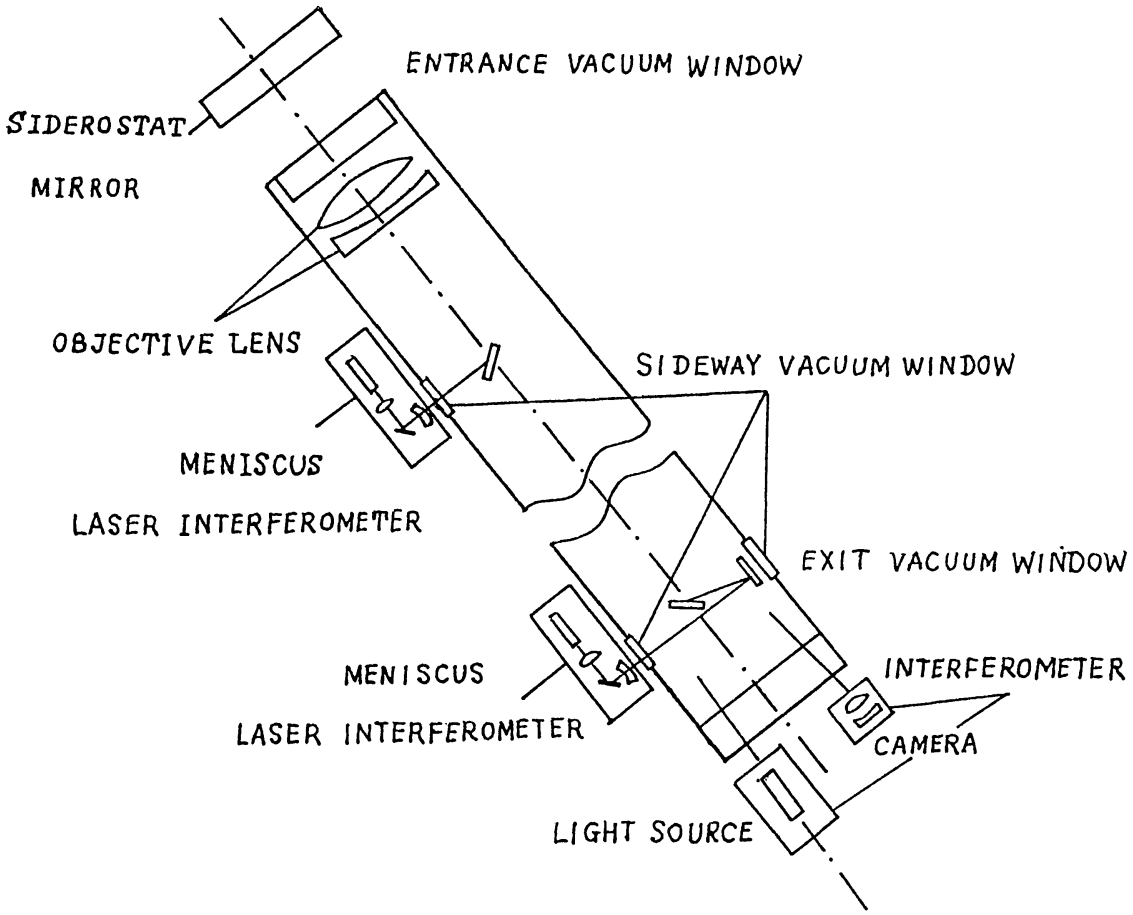


Fig. 6. Layout of the interferometers to test the optical system in real time.

Fig. 7. Interference between the two surfaces of the entrance window.

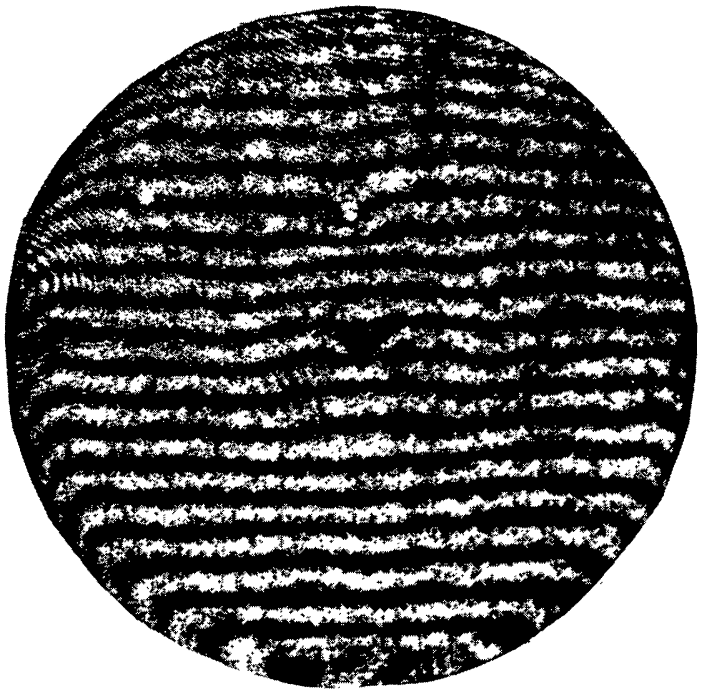

Fig. 8. Double-pass interferogram of the entrance window.

interference pattern. In Figure 7 one can see such interference corresponding to small temperature gradients. The figure of the one surface of the window and its optical wedge are responsible for such a curious pattern. We can compare two interference patterns: one is the wavefront of the beam that has passed through the glass window and was taken in the laboratory (Figure 8), and the other is the interference between two surfaces of the same window (Figure 7). The observer can make an interference pattern, Figure 7, in real time simultaneously with the solar image and control the temperature regime of the entrance illuminator. Under exposure to solar radiation and with a change in ambient temperature, the metal mount of the entrance window is heated up and cooled down faster than the glass. This gives rise to temperature gradients at the entrance window. A ring thermostat was installed to keep the temperature on the side of the entrance window close to that at the center of the window. Gradients on the lenses are ten times less than on the window because the vacuum tank with a double wall protects the lenses against ambient temperature variations, and the lens mounts are enclosed to protect them against the solar radiation.

The middle focal plane interferometer was installed to monitor the surface of the flat siderostat mirror and its supporting system. The interferometer uses the autocollimation image reflected by the siderostat mirror and formed with the objective like a collimator.

## 4. The Pneumo-Mechanical Axial Support System

When tracking the Sun, the angle of inclination of the siderostat mirror can change its sign with respect to the vertical during the daytime. We have designed a new effective version of the axial support that operates with both negative and positive angles of inclination of the mirror.

Let the mirror be placed in the horizontal position on evenly distributed balancing Grebb's supports and faced up (positive angle of inclination). Between the backside surface of the mirror and the mount there is a hermetic volume. The mirror presses on supporting points by its own weight. We do not reduce the weight pressure of the mirror by pumping air into the volume. Now we tilt the mirror. The pressure on the support is reduced. Therefore, we create a partial vacuum to get the same pressure as in the horizontal position. We continue tilting the mount with the mirror and increasing vacuum according to the cosine rule. When the mirror is in the vertical position, the force of pressure on the support is equal to the weight of the mirror. In the case of a negative angle of inclination the vacuum grows continuously depending on the angle. When the mirror is in the horizontal position with its face down, the additional outside pressure not only compensates the weight of the mirror but also presses it, giving the same pressure on the support as in the very beginning. So the normal force acting on the surface mirror should be

$$N = G + G\cos\alpha = 2G\cos^2\alpha/2\,, \tag{1}$$

where $G$ is the weight of the mirror, $\alpha$ is the angle between the mirror-face normal and the nadir direction. To satisfy the condition (1), the pressure is reduced by the value

$$\rho = \frac{2G}{S}\cos^2\alpha/2\,, \tag{2}$$

where $S$ is the area of the mirror. The construction realizing such change in pressure looks like a cosine mechanism (Aleksandrovich *et al.*, 1990).

The edge of the mirror slides slightly on the rubbery rolls of the radial support. One side of the sealing belt cuff is attached to the glass, and the other to the ring. The cuff preserves a gap between them. Because the gap is very narrow, the cuff does not press and deform the mirror edge. The range of air pressure in the volume is less than atmospheric pressure by 30–60 mm mercury.

The first succesful interferograms were taken after the support system had operated well. The interferogram of the optics, the whole telescope in the autocollimation scheme with the siderostat mirror, and the map of the wavefront are presented in Figures 9 and 10. Distortions of the interference fringes are connected with the zonal and local figure. The round spot is the result of a glass bubble. Table I contains the optical parameters (in waves) taken under ideal warm gradient

Fig. 9. Optical system double-pass interferogram.

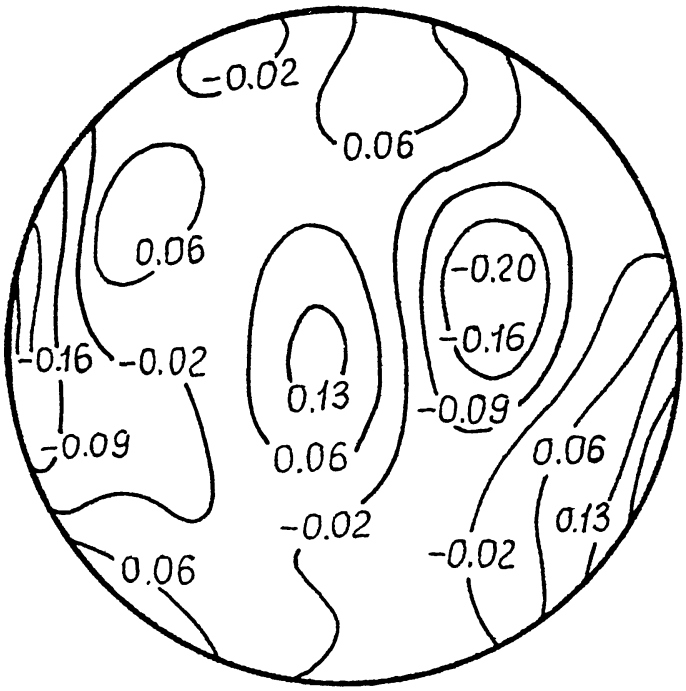


Fig. 10. Wavefront of the whole optical system.

TABLE I
Characteristics of the optical system

| System elements | r.m.s. deviation | Astigmatism | Coma | Strehl number |
|---|---|---|---|---|
| Objective lens | 0.06 | 0.10 | 0.11 | 0.88 |
| Objective lens + window (calculation) | 0.08 | 0.06 | 0.31 | 0.79 |
| Objective lens + window + mirror | 0.08 | 0.05 | 0.37 | 0.78 |

conditions. The parameters of the entire telescope look good, because of some compensation of the different element distortions. The birefringence of the optical system has an axial symmetry and reaches its peak $0.25\lambda$ in the edge.

The dome, which is above the siderostat, produces some warm air. We need to change the tower construction to put it farther away from the siderostat. Of course, if we use a new athermal glass for the entrance window, the thermal condition will be more uniform. Presently, the optics of the telescope are in accord with Rayleigh's criteria if the temperature gradient is no more than 0.3 C.

## 5. The Spectrograph and an Illustration of First Spectral Observations

For purposes of enabling a wide class of spectrographic and magnetographic research of the solar and terrestrial atmospheres, the telescope is equipped with a spectrograph. The requirements for the spectrograph are dictated by the purpose of the telescope and are as follows: the spectrograph should not reduce substantially the high spatial resolution with good spectral resolution.

The spectrograph embodies the horizontal Ebert design, but it includes two moving camera mirrors. The dispersion device is a $200 \times 300$ mm, 600 lines $\text{mm}^{-1}$ diffraction grating with a blaze angle of 53°.

The spectrograph-telescope facility has the best performance when the aperture ratios of the telescope and spectrograph are the same. The dimensional design of the spectrograph was dictated by the aperture ratio of the telescope, $f/53$, and by the vertical size of the grating.

Figure 11 presents the spectrograph design: S – spectrograph slit; G – diffraction grating; M – collimator ($D = 283.5$ mm, $f = 9.5$ m); M1 and M2 – camera mirrors ($D1 = 598$ mm, $D2 = 603$ mm, $f1 = f2 = 14$ m); K is the cassette part. The mirrors are all made of glass ceramic. The foundation supporting the camera mirrors has rails to enable the mirrors to translate within 5 m. When two camera mirrors are used simultaneously, the spectrum from the second camera mirror enters the cassette placed above the first. $\alpha_{1,2,3}$ are the angles of incidence of the beams on

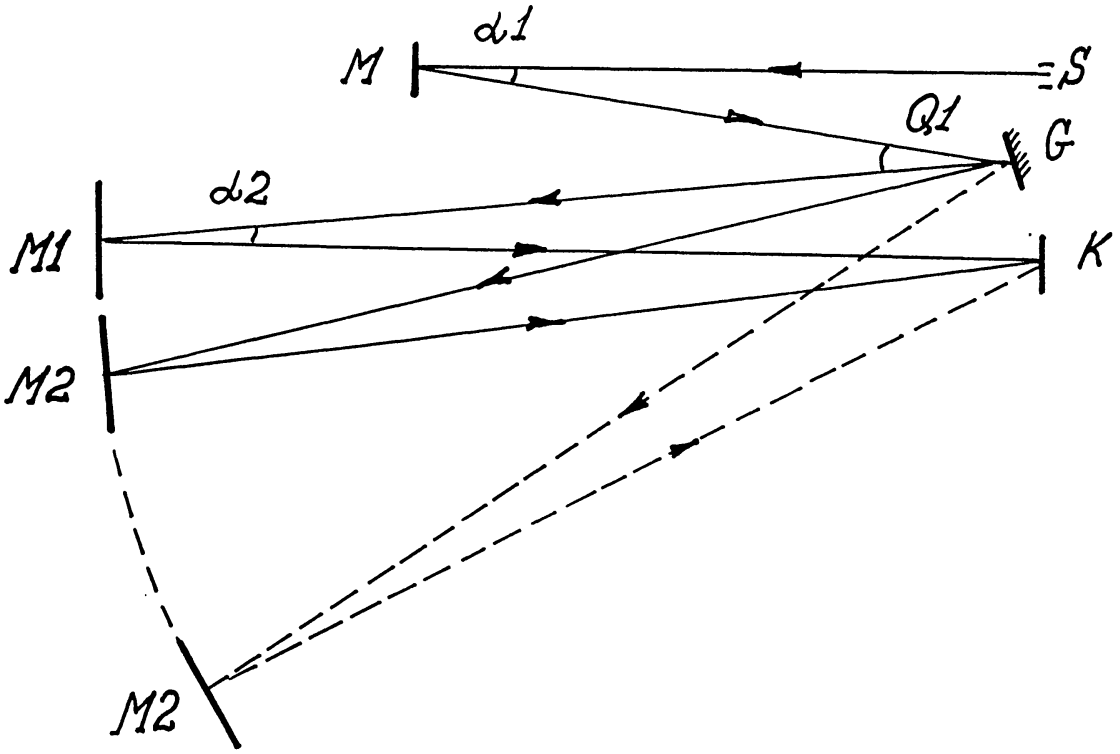


Fig. 11. The spectrograph design. On this figure the vertical scale is extended 5 times compared with the horizontal scale.

the mirrors, and $Q$ is that of the grating. The minimum angles at which the system is free from vignetting are: $\alpha_1 = 1°05'$, $\alpha_2 = 1°21'$, and $Q = 2°22'$ (Firstova, 1980).

The spectrograph aberrations include the total action of the collimator and camera mirror aberrations, where the principal contribution is made by spherical aberrations and the third-order coma, as well as by off-axis aberrations introduced by the absence of the axial symmetry of the Ebert system. The total aberration spot on the intersection of the gaussian plane with the horizontal plane passing through the slit center, has the size

$$\delta y = -0.0008\,\text{mm}\,, \qquad \delta z = +0.0292\,\text{mm}\,, \tag{3}$$

which indicates an aberration-free system in the dispersion ($y$ direction). In the direction of the spectrograph slit ($z$ direction), the aberration effect reduces the theoretical spatial resolution by at least $0.1''$.

Focusing of the collimator and the camera mirrors is done using a mercury lamp visually by means of the Foucault knife and photographically. For small rotational angles of the grating (lower orders), there is almost no astigmatism; however, for angles close to the blaze angle of 53°, the difference in sagital and meridional foci is 28–30 mm, thus corresponding to 0.2% of the focal length of the camera mirror (Firstova, Gubin, and Lankevich, 1990).

TABLE II

Spectral characteristics of the diffraction grating

| $K$ | $\Delta\lambda$ (Å) | $\Delta\lambda_{max}$ (Å) | $d\lambda/dl$ (Å mm$^{-1}$) | $\Delta\lambda_{obs}$ (Å) | $R$ (G) | $R$ (Sp) | $R$ (G)/$R$ (Sp) |
|---|---|---|---|---|---|---|---|
| 1 | 5000 | 26720 | 1.17 | | 147541 | | |
| 2 | 2500 | 13360 | 0.56 | 0.029 | 295082 | 221259 | 0.75 |
| 3 | 1670 | 8910 | 0.35 | 0.022 | 442623 | 286335 | 0.65 |
| 4 | 1250 | 6680 | 0.23 | 0.016 | 590164 | 385854 | 0.64 |
| 5 | 1000 | 5340 | 0.16 | 0.011 | 737705 | 585926 | 0.79 |

The principal spectral characteristics of the grating appear in the first four columns of Table II: $K$ is the order of the spectrum; $\Delta\lambda$ is the dispersion region centered on $\lambda$5000 Å (which is the value of a spectral interval in which the spectrum of a given order does not overlap with spectra of neighboring orders); $\Delta\lambda_{max}$ is the region of maximum energy concentration in a given order; and $d\lambda/dl$ is the value of the inverse linear dispersion.

The spectrograph instrumental profile was determined photographically from the fine structure of the green line 5460.7 Å of the mercury lamp and from the line 6328 Å of the helium–neon laser. The image size from the light source on the collimator corresponded to the operating conditions (200 mm). The 5–40 s exposure time interval has regions of underexposure and overexposure. No grating ghosts were detected, even in the case of the longest exposures. The fifth column of Table II shows the observed values of the line width $\Delta\lambda_{obs}$, in the 6328 Å line. The sixth column gives the values of the theoretical resolution of the grating, $R$ (G), as obtained from

$$R(G) = \frac{1}{122} KNW = \frac{1}{1.22} \lambda/\delta\lambda \,, \tag{4}$$

where $N$ is the number of grating rules per mm, $W$ is the total grating length, and $\lambda/\delta\lambda$ is a theoretical resolution limit. The divisor 1.22 is due to the fact that the beam's cross-section on the grating is not a rectangular one, because the beam is inscribed in the grating and does not fill it up. On substituting into expression (4) the half-width value of the instrumental function $\Delta\lambda_{obs}$ from Table II we obtain the value of actual telescope resolution $R$ (Sp).

The last column shows the ratio of the spectrograph actual resolution to the theoretical resolution of the grating. According to Dervis (1985), the ratio of spectrograph to grating theoretical resolution corresponds to the value $\approx$ 0.7. Thus, we can conclude that the actual resolution of the spectrograph is consistent with the theoretical one.

The spectrograph characteristics obtained allow one to employ it for solving relevant problems in solar physics of investigating the fine and superfine structure of

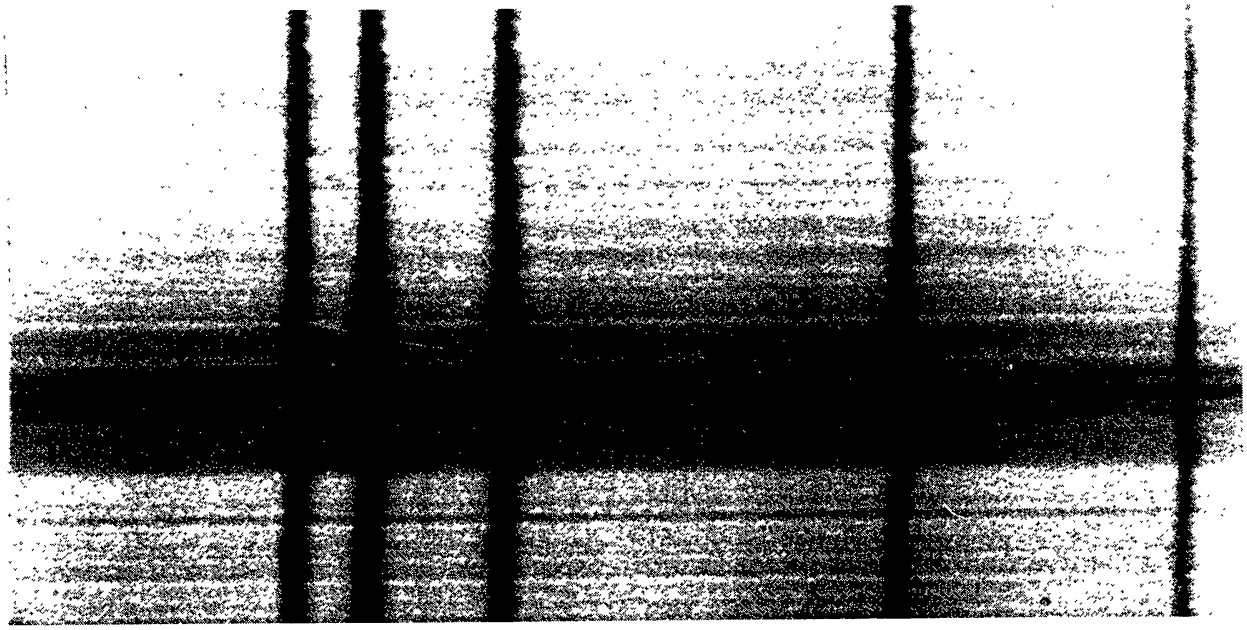

Fig. 12. A sunspot spectrogram in the region 6173 Å.

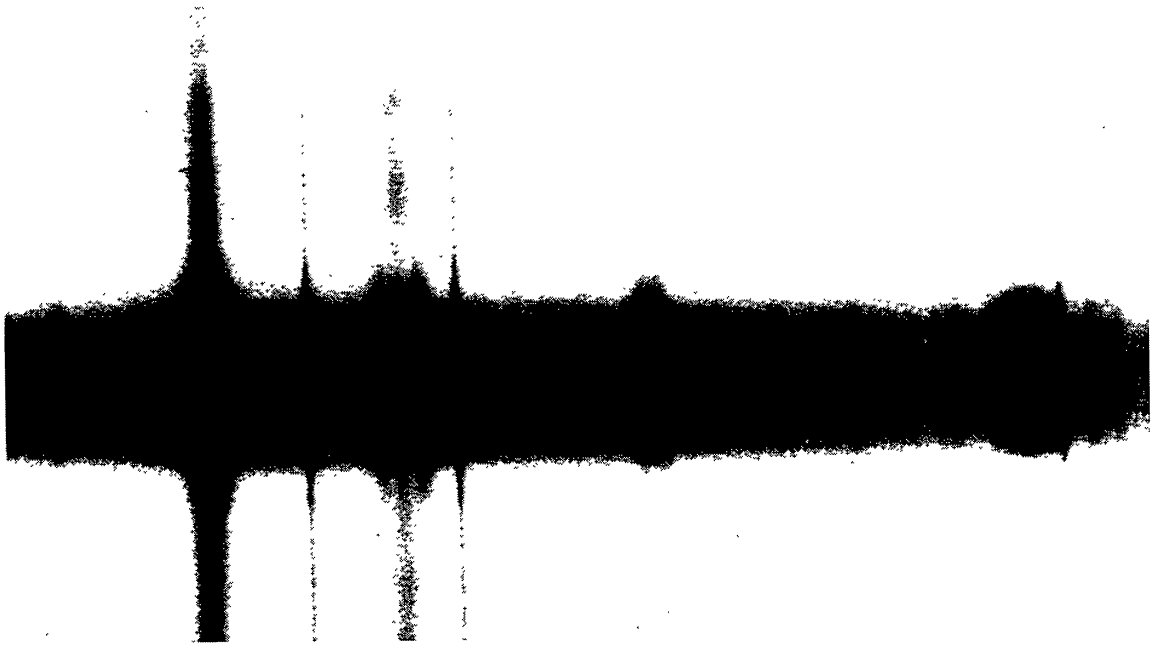

Fig. 13. A composite sunspot spectrogram in the 6303 Å line.

spectral lines. To illustrate the spatial and spectral resolutions of the telescope, Figures 12–14 present spectrograms obtained with the Large Solar Vacuum Telescope. Theoretical spatial resolution is not achieved in the spectrograms presented. The new suppot system of the mirror and the temperature control of the entrance window (the description in this paper) will hopefully improve the quality of images.

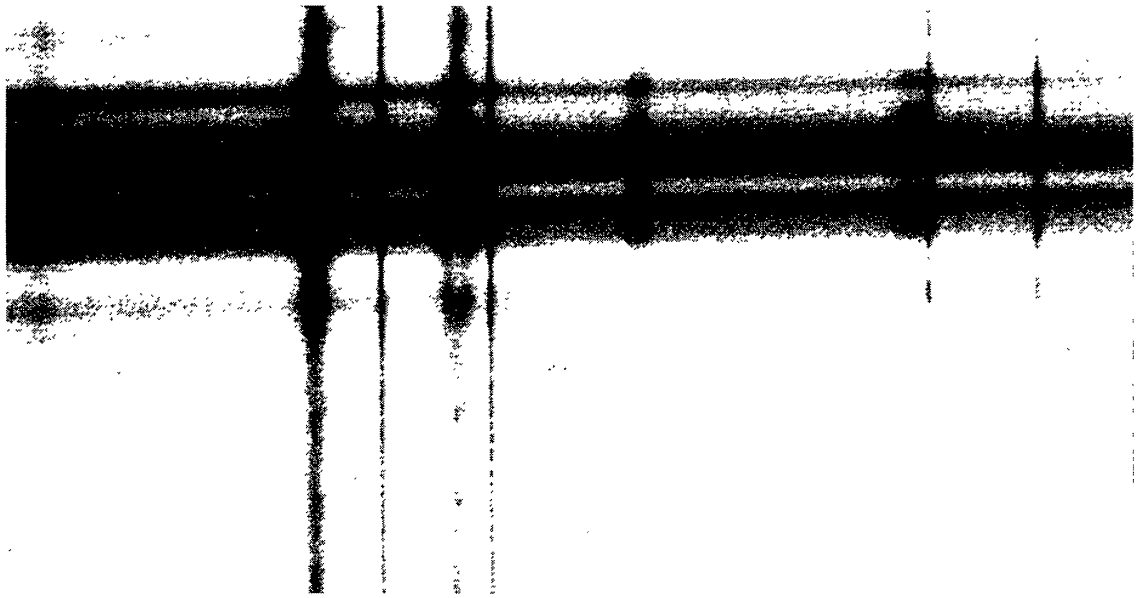

Fig. 14. The fine structure of the Doppler velocity field in Fraunhofer lines in the spectral region 6303 Å.

## 6. Conclusion

The Large Solar Vacuum Telescope (LVST) with a spatial resolution of 0.3″ of arc complies with modern requirements for ground-based instruments in regard to spatial and spectral resolutions and provides high-dispersion spectra of fine-structured solar features.

## Acknowledgements

It is our great pleasure to mention that G. N. Domyshev designed the test instrument and fabricated the optics, P. G. Kovadlo, N. A. Lankevich, A. V. Gubin, and I. B. Maksiutov made the entrance window thermostat, S. V. Aleksandrovich, V. P. Kvacheva, and V. I. Kruglov took part in designing the support system, and Yu. A. Klevtsov calculated optico-physical parameters. We wish to acknowledge the efforts of our colleagues whose article we have used here.

## References

Aleksandrovich, C. V., Domyshev, G. N., Kvacheva, V. N., Kruglov, V. I., and Skomorovsky, V. I.: 1990, *Bull. Izobretenii* **7**, Inventors Certificate 1580310.

Dervis, T. E.: 1985, *Astronomical Spectrographs*, Leningrad, p. 84.

Domyshev, G. N., Klevtsov, S. A., Skomorovsky, V. I., Gan, M. A., and Ustinov, S. I.: 1982, *Issledovaniya po geomagnetizmu, aeronomii i fizike Solntsa* **60**, 212.

Firstova, N. M.: 1980, *Issledovaniya po geomagnetizmu, aeronomii i fizike Solntsa* **52**, 122.

Firstova, N. M., Gubin, A. V., and Lankevich, N. A.: 1990, *Issledovaniya po geomagnetizmu, aeronomii i fizike Solntsa* **91**, 166.
Kruglov, V. I., Shamsutdinov, M. A., Kitov, A. K., Kuznetsov, Yu. A., Grigoryev, V. M., and Govorukhin, V. Ya.: 1980, *Issledovaniya po geomagnetizmu, aeronomii i fizike Solntsa* **52**, 76.
Stepanov, V. E., Banin, V. G., and Kruglov, V. I.: 1979, *Novaya tekhnika v astronomii* **6**, 42.